

Analysis of wave band gaps in mechanical metamaterial based on Nelder–Mead method



Jiaqi Dong, Weiqi Chen, Zhe Zeng, Qing-Hua Qin*, Yi Xiao

Research School of Engineering, Australian National University, Acton, ACT 2601, Australia

ARTICLE INFO

Keywords:

Optimization algorithm
Mechanical metamaterial
Nelder–Mead method
Wave band gap
FEA simulation

ABSTRACT

One of the fundamental challenges in engineering design of an elastic metamaterial is optimizing its structure in a fine but controllable geometry based on a performance criterion. In this study, the wave manipulation ability of the metamaterial is taken as the key criterion for the optimization of its unit structure governed by the changing geometric parameters. The complete dispersion relationship of the metamaterial is set as the performance criterion which is acquired by scanning the wave vector k along the contour of the irreducible Brillouin zone in the reciprocal space for the unit cell and evaluating its eigenfrequency values in different eigenmodes. For the optimization algorithm, the Nelder–Mead method is programmed in the form of MatLab scripts incorporated with tailored parameter ranges to ensure geometric compatibility and a finite element analysis (FEA) solver for eigenfrequency evaluation. Parametric optimization is conducted for 100 iterations where promising convergence is observed. The optimized geometry is then compared to the initial in its performance. In all three case studies, including planar and spatial lattices, the optimized geometry showed superior properties and larger complete band gaps. The Nelder–Mead method is proved to be an effective tool for metamaterial optimization.

1. Introduction

Over the past two decades, research on mechanical metamaterial structures has gained high level of interest from academics and industrial stakeholders globally due to their capabilities to bring novel multifunctionalities. Some of the examples include locally resonant sonic materials [1], soft metamaterials with negative Poisson's ratio [2], dilational elastic metamaterials [3], ultra-lightweight lattices [4,5], and pentamode mechanical metamaterials [6]. Elastic wave propagation under local resonant is one in the main streams of mechanical metamaterial research. For instance, in 2007 Fokin et al. established a systematic approach to retrieve effective properties of a locally resonant metamaterial made from a homogeneous fluid slab of material [7]; in 2014 a group of researchers provided both theoretical and experimental analysis on forming new three-dimensional metamaterial structures using the principles of origami art [8]; in 2016, Wang et al. [9] demonstrated successful wave manipulation both theoretically and numerically by incorporating lateral local resonator in a traditional beam model. The manipulation can also be achieved by other methods. For example, Chang et al. [10] demonstrated a pre-deformed Neo-Hookean material can behave like a smart metamaterial and can be utilized to manipulate both in-plane and anti-plane S-waves.

The geometrical arrangement of these metamaterials greatly affects their properties. Three-dimensional dilational structures, for instance, are a family of mechanical metamaterials that display chirality through wave refraction. An initial geometry, proposed by Buckmann et al. [3], was specified with four independent geometrical variables. Strategically varying these variables based on repeated performance tests gives potential to parametrical optimization of its geometry. The structural design drew inspiration from an analogy to the previous electro-magnetic metamaterial structure with coils and split-ring resonators arranged periodically to produce local resonance [11]. Following the discovery, a group of structures emerged with similar rotating arrangement of rods surrounding a dense core which propelled the research on metamaterial structures and inspired scientists to seek more innovative vibration modes that exhibits the property [12–14].

The metamaterial performance of these original designs can often be optimized by manipulating the unit cell geometry. Traditionally this is completed by a manually analytical approach specific to the design itself, especially for 3D unit structures, which is not widely applicable [15,16]. In this work an automatic approach is established to numerically optimize the geometrical design. The approach is then examined in three scenarios. The success in all scenarios indicates a general applicability of this approach to various metamaterial design problems.

* Corresponding author.

E-mail addresses: jiaqi.dong@anu.edu.au (J. Dong), u5423569@anu.edu.au (W. Chen), u5893134@anu.edu.au (Z. Zeng), qinghua.qin@anu.edu.au (Q.-H. Qin), yi.xiao@anu.edu.au (Y. Xiao).

On the other hand, the prosperity of mechanical metamaterial theories spawned various geometric designs and physical implementations. Many researchers have achieved promising outcomes using innovative manufacturing methods to create composite structures that exhibit metamaterial properties. In 2004, Yang et al. [17] pioneered the field by fabricating a three-dimensional phononic crystal with tungsten carbide beads surrounded by water. Following these trials, more and more researchers have made their own rendition of metamaterial manufacture [18–21]. However, most of these designs left room of improvement in their performance. And such could be easily achieved with structural optimization.

Among structural optimization methods, topology optimization is one of the most popular. Applications of topology optimization have attracted a great amount of attention in recent years [22–24]. However for this study the Nelder–Mead method is chosen for programming the optimization algorithm. Being one of the most widely used optimization methods, it belongs to the family of numerical methods, which offers simplicity and precision in calculation without the need for evaluating integrals [25–27]. The Nelder–Mead method utilizes a simplex, depending on the number of dimensions of the parameter domain, with each index representing a trail configuration to seek an optimal solution over iterations. Groups of indices are produced by generation, with each of them being superior in performance to the previous one. The details of the method are discussed in the following section.

Parametric optimization methods are preferred over topology optimization due to the fact that the structural designs resulted from topology optimization often contain highly irregular angles and surfaces. Structures produced by topology optimization methods are also more difficult to replicate on a different scale, which is often required with mechanical metamaterials. In comparison, parametric optimization takes advantage of a pre-existing arrangement of structural components, changing the geometry by only altering the governing parameters. Hence the optimized geometry can be produced in a similar approach to the original. Also the Nelder–Mead method used in this work is particularly good at handling a large number of variables which makes it possible to expand the findings to a higher-degree domain of variables [28,29].

As the mechanical metamaterials examined in this work are derived from simple two-dimensional designs, their geometry patterns are entirely defined by only a handful of parameters. A small change of these could render a great impact on their performance. Therefore parametric optimization is often sufficient in investigating these simpler structures. Lastly, parametric optimization methods are largely numerical, indicating a void of differential analysis. This helps accelerating the optimization process, making it suitable for implicit problems.

2. Methodology

Due to the complex of unit geometry, in this work we evaluate the performance of a mechanical metamaterial by means of numerical simulation with FEA [30–33]. The FEA solver is employed to search for eigenfrequencies of the model subject to a wave vector with various spatial frequencies. When a complete isolation forms between two eigenmode curves, the eigenfrequency margin between them indicates maximum attenuation of the incident wave. Such phenomenon is defined as an elastic band gap. To accurately analyze the performance of the metamaterial, a complete dispersion relation is investigated. Quintessentially, the wave vector scans across the entire first Brillouin zone in the reciprocal space, which can be reduced to the irreducible Brillouin zone. Here we investigate both two-dimensional square and three-dimensional cubic models with different Brillouin Zones by controlling the wave vector, \vec{k} .

Their dimension of the reciprocal lattice can be calculated with respect to the dispersion relationship by:

$$k_{max} = \frac{\pi}{a},$$

Table 1

Corresponding formulation of each operation, where α , β , σ_1 , σ_2 and δ are coefficients. In this study a standard configuration is used, where: $\alpha = 1$, $\beta = 2$, $\sigma_1 = \sigma_2 = \delta = 1/2$.

Operation	Formulation
Reflection	$x_R = \sum_{i+1}^n x_i + \alpha \left(\sum_{i+1}^n x_i - x_W \right)$
Expansion	$x_E = \sum_{i+1}^n x_i + \beta \left(\sum_{i+1}^n x_i - x_W \right)$
Outer-contraction	$x_{OC} = \sum_{i+1}^n x_i + \sigma_1 \left(\sum_{i+1}^n x_i - x_W \right)$
Inner-contraction	$x_{IC} = \sum_{i+1}^n x_i - \sigma_2 \left(\sum_{i+1}^n x_i - x_W \right)$
Shrink	$x_{i,shrunk} = x_B - \delta(x_i - x_B), i = 2, 3, \dots, n + 1$

where a is the unit cell length in physical space, and the resultant maximum wave number k_{max} is half of the side length of the first Brillouin Zone. By optimizing the performance of a mechanical metamaterial, the band gap can be tailored to be more suitable for its application. As a metamaterial structure can be easily scaled in dimension which leads to shifting of the band gap position proportionally, the sole interest of this study is the enlargement of band gaps.

Keeping the main goal of optimization in mind, the objective is derived: to increase the relative width of the primary bandgap. The objective function can be expressed as:

$$\text{Maximize: } \bar{d} = \frac{(f_{upp_min} - f_{low_max})}{\frac{f_{upp_min} + f_{low_max}}{2}}; \text{ Subject to: } f_{upp_min} - f_{low_max} > 0.$$

In this case the relative band gap width is defined as the ratio of the absolute gap width, calculated by taking the distance from the highest point on the lower eigenfrequency curve and the lowest point on the higher one, to the median frequency of the gap, which determines its position on the spectrum. As the model geometry is scaled, the frequency graph is scaled proportionally, both in position and in width. By measuring the relative gap width the effect of scaling is eliminated so the objective reflects the true width of the gap.

Implementing the objective shown above, an optimization algorithm can be built using the Nelder–Mead method. Mathematically, new points are generated based on the coordinates of the previous indices. These operations are expressed as follows, with the coordinates denoted as \vec{x} . Here the number of indices is $n + 1$, with point W ranked at the last place ($i = n + 1$) and point B ranked first ($i = 1$). The generation of new points follows the mathematical formulation shown in Table 1.

Termination conditions in this case include a limit on the number of iterations as well as a minimum deviation between the indices. The maximum number of iteration is set to be 100 generations, while a strict

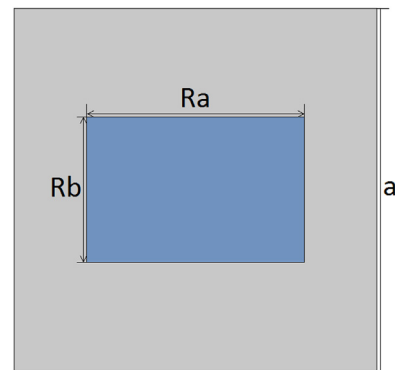


Fig. 1. Two-dimensional phononic crystal geometry. (For interpretation of the references to color in this figure, the reader is referred to the web version of this article.)

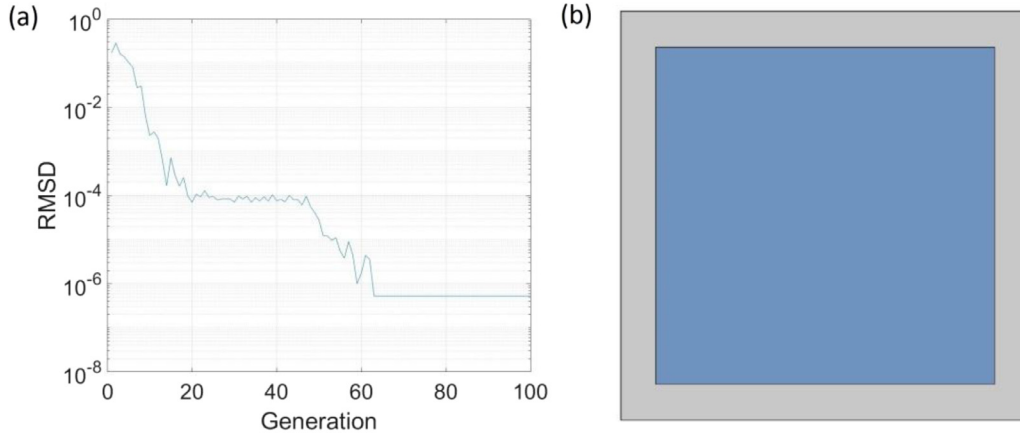


Fig. 2. (a) RMSD plot shows rapid convergence and (b) Final geometry with enlarged core. (For interpretation of the references to color in this figure, the reader is referred to the web version of this article.)

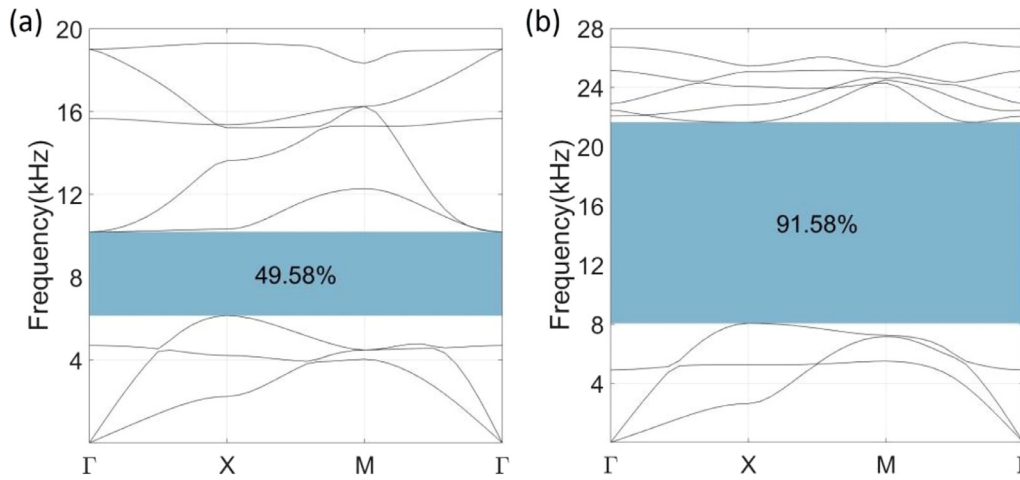


Fig. 3. (a) Initial band structure where $R_a = R_b = 0.6 \cdot a$. (b) Optimized band structure where $R_a/a = 0.82879$ and $R_b/a = 0.82386$.

deviation threshold is set: $RMSD_{min} = 1 \cdot 10^{-6}$. Upon reaching either one of the conditions the program will exit the loop and return all data.

$$RMSD = \sqrt{\frac{\sum_{i=1}^n (\bar{x}_i - x_i)^2}{n}}; \text{ where } \bar{x}_i = \frac{\sum_{i=1}^n x_i}{n}.$$

In this study, the optimization process is conducted by combining MatLab scripts which analyze the results and execute the NM algorithm, with a FEA solver that provides simulation data given the generated sets of parameters. The data is then transmitted to the MatLab program and the objective value is extracted for each of the indices. With three-dimensional simulations the model is built as a cubic representative volume element. Considering the Bloch’s theorem, with the representative volume element, periodicity conditions are applied to the three pairs of sides to satisfy the following relationship:

$$\psi(\mathbf{r}) = e^{i\mathbf{k} \cdot \mathbf{r}} u(\mathbf{r}).$$

Due to the numerical nature of simplex optimization methods, the geometrical compatibility needs to be programmed individually into the algorithm before analyzing each design. Triangular and tetrahedral elements are used, respectively, for two-dimensional and three-dimensional models, with quadratic Lagrange interpolation between nodes to enhance accuracy. The outcomes from each simulation are shown in the following section.

3. Results

3.1. Shape optimization of two-dimensional phononic crystal

For the two-dimensional validation of the algorithm, a square phononic crystal is examined. The geometry is governed by three parameters, namely internal length R_a , internal height R_b , and the edge of cell $a = 0.1 \text{ m}$ exhibited in Fig. 1. As can be observed the structure is composed of two different materials: the core, shaded in blue and the matrix in grey. Both matrix and core materials are virtual homogenous materials with the following characteristics:

Material 1 (matrix): $E_1 = 2GPa$; $\rho_1 = 1 \cdot 10^3 \text{ kg/m}^3$; $\gamma_1 = 0.45$.

Material 2 (core): $E_2 = 200GPa$; $\rho_2 = 8 \cdot 10^3 \text{ kg/m}^3$; $\gamma_2 = 0.34$.

The shape optimization is conducted by altering the geometric parameters R_a and R_b . They are in proportion to the cell length, so the primary variables of interest are the ratio of R_a and R_b to a individually, which forms a two-dimensional parametric domain. The simplex in the two-dimensional domain is a triangle. Utilizing the NM method, the program will generate three indices for the initial simplex, then shift the indices across the domain, and gradually approach a simplex corresponding to a peak value of the optimization objective.

For quicker computation we included at the start of the NM algorithm a seed geometry ($\frac{R_a}{a} = \frac{R_b}{a} = 0.6$) to ensure a valid complete band gap from input. In the nature of Nelder–Mead parameter search, the method does not require a successful seed input. However random

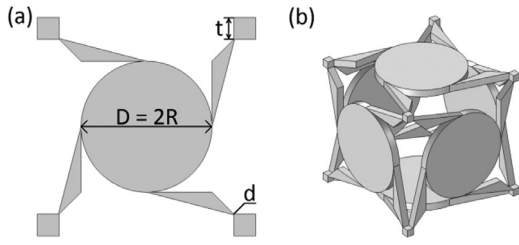


Fig. 4. (a) Planar view of dilational metamaterial structure. (b) Initial seed geometry where $R = 0.3a$, $t = 0.1a$ and $d = 0.004a$.

search without the seed geometry may lead to slow convergence and significantly higher consumption of computational power. The inclusion of seed geometry is particularly desirable with three-dimensional models as the number of degrees of freedom increases drastically.

As shown in Fig. 2(a), convergence occurs very rapidly in the latter case (purple curve). The relative bandgap width increases drastically and reaches optimum within the first 12 generations. Inspired by the two-dimensional scenario, the following cases are studied with the same techniques.

As presented in Fig. 2(b), the final optimized geometric parameters are:

$$\frac{R_a}{a} = 0.82879; \frac{R_b}{a} = 0.82386.$$

The initial and optimized band structures are shown in Fig. 3. The final gap width is 91.58%. Compared to 49.58% initially, the bandgap is

improved by 84.71%. The total time elapsed for this procedure is 28 min. This method proved to be effective in optimizing two-dimensional patterns that possess unique properties of metamaterials.

3.2. Shape optimization of three-dimensional dilational PC cell

Following the previous two-dimensional trial, a three-dimensional dilational metamaterial structure is investigated. The initial geometry and band structure are displayed in Fig. 4. In this case the geometry is governed by three parameters: t , d and R . R stands for the radius of the circular core; t represents the thickness of the plate when the three-dimensional cell is constructed by extruding and combining the two-dimensional drawing; and d stands for the width of the connection branch. Once more the cell geometry is in proportion to the overall length a (abbreviation since irrelevant), which also contributes to the determination of wave vector \vec{k} , and the position of all bands on the spectrum.

For this scenario a brief trial is conducted for 20 iterations and good convergence is reached rapidly. The number of twenty iterations was selected due to high consumption of computational power with three-dimensional models. Moreover the three-variable case was not the main emphasis of the project rather than the four-variable case which includes direct relevance to the previous work by Buckmann et al. [3]. An extended investigation of this geometrical design will be conducted in an upcoming project where the shape will be studied in greater details and more iterations of optimization.

Same as previous, the minimum RMSD is set to 1×10^{-6} . The initial geometry yields a band structure where no complete gap can be found.

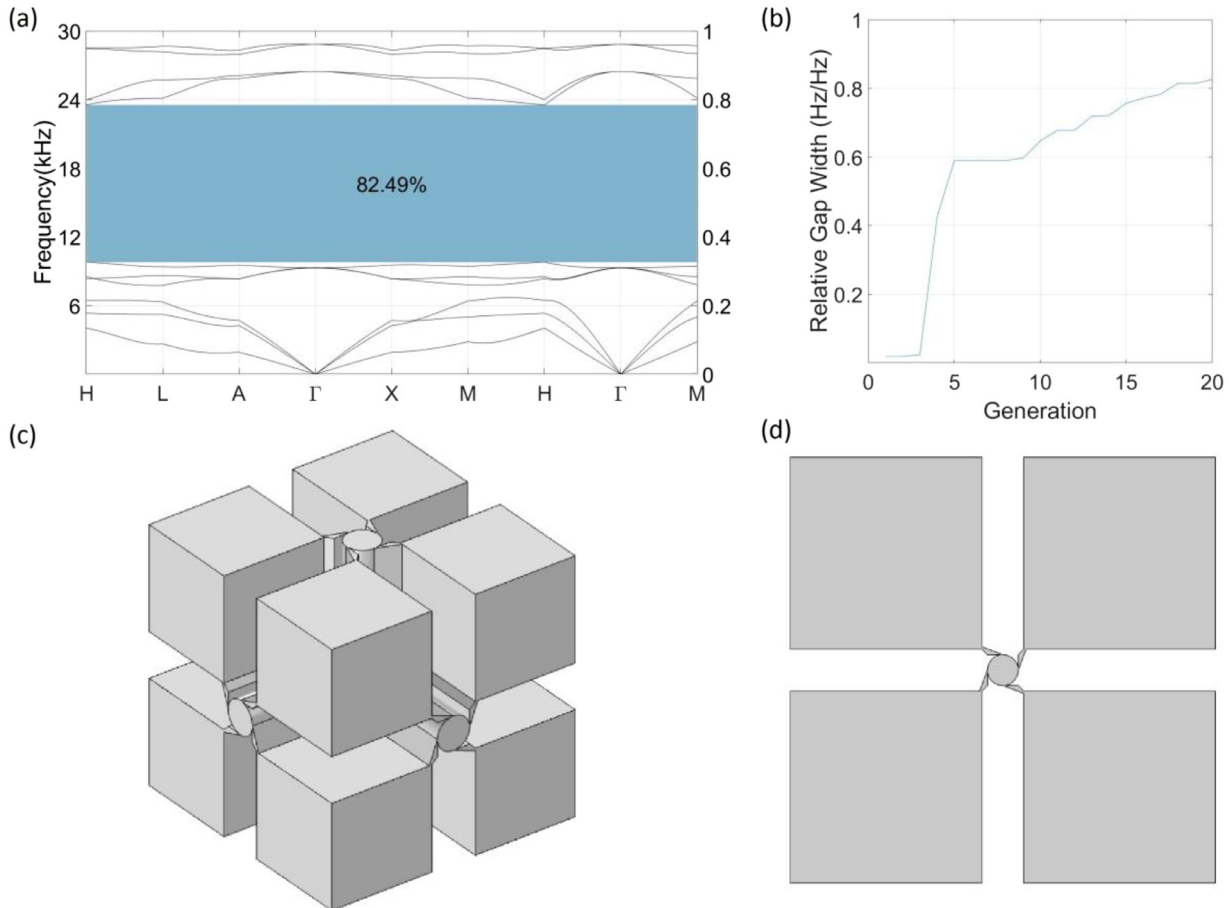


Fig. 5. (a) Optimized band structure showing a primary gap width of 82.5%. (b) Convergence plot indicates rapid convergence in first 20 iterations. (c) and (d) Optimized geometry and three-dimensional cell structure.

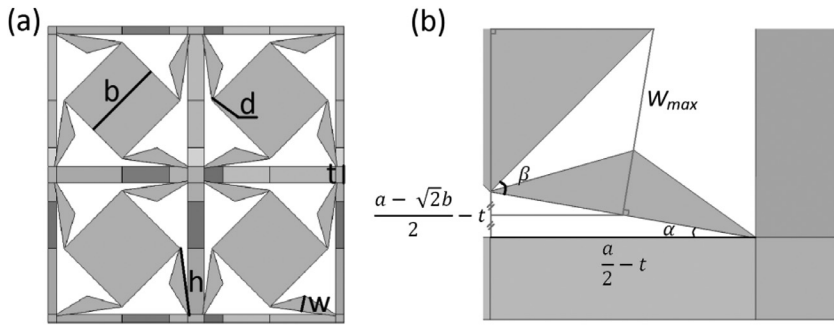


Fig. 6. (a) Initial dilational metamaterial structure. (b) Consideration of the geometrical compatibility of the parameters.

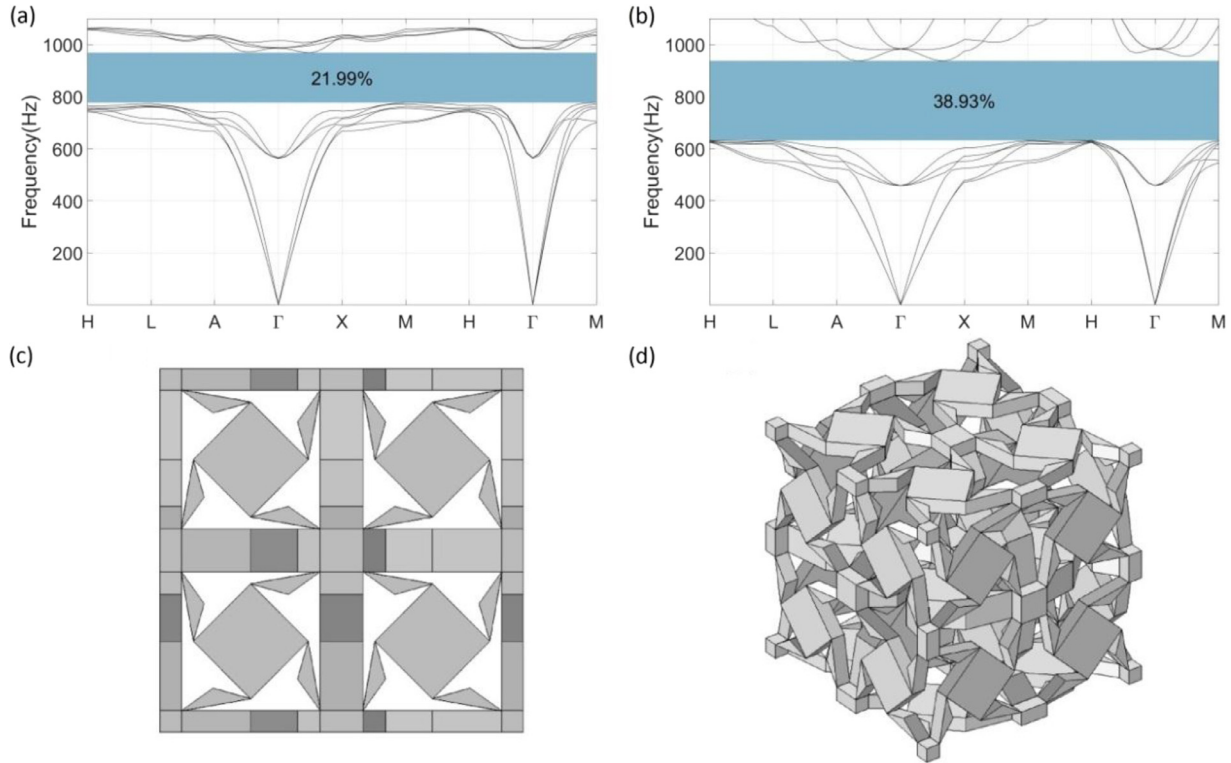


Fig. 7. (a) Initial band structure. (b) Optimized band structure with widened gap. (c) Optimized two-dimensional geometry. (d). Isometric view of optimized structure.

After the optimization procedure, the final parameters are as follow:

$$\frac{R}{a} = 0.03634; \quad \frac{t}{a} = 0.45086; \quad \frac{d}{a} = 0.00551.$$

As illustrated in Fig. 5, the optimized structure is greatly deformed in shape as compared to the original. The nodes (of side-length t) are significantly enlarged while the core diminished. The resultant band structure displays a complete gap between the sixth and seventh bands, and the final gap width is 82.5%.

3.3. Four-variable shape optimization of pre-existing metamaterial structure

The trial reveals potential of creating novel structures with large band gaps using numerical optimization methods. With interest in improving the performance of pre-existing three-dimensional mechanical metamaterial structures, a three-dimensional dilation metamaterial structure, proposed by Buckmann et al. in 2014 [3], is investigated. Shown in Fig. 6 is the initial geometry, determined by a series of shape parameters, all in proportion to cell length a . As h is driven by the rest of the parameters only b (B^*a), d (D^*a), t (T^*a) and w (W^*a) are considered. A four-variable parametric domain is therefore generated.

With the complicated structure it becomes vital to define a realistic range for all geometric parameters to avoid overlapping. The parameters must be varied within ranges compatible with each other. Considering the geometry, the following calculations are made:

$$\tan(\alpha) = \frac{\frac{a}{2} - \frac{\sqrt{2}}{2}b - t}{\frac{a}{2} - t};$$

$$\alpha = \arctan\left(\frac{\frac{a}{2} - \frac{\sqrt{2}}{2}b - t}{\frac{a}{2} - t}\right) = \arctan\left(\frac{1 - \sqrt{2}B - 2T}{1 - 2T}\right); \quad \beta = \alpha + \frac{\pi}{4}$$

$$w_{max} = \frac{\tan(\beta)}{2} * \frac{\frac{a}{2} - \frac{\sqrt{2}}{2}b - t}{\sin(\alpha)} = \frac{\tan(\alpha) + 1}{2 - 2\tan(\alpha)} * \frac{\frac{a}{2} - \frac{\sqrt{2}}{2}b - t}{\sin(\alpha)}.$$

So the definitive ranges of the parameters are:

$$W \in [0.05, 0.4]; \quad T \in [0.1, 0.5]; \quad B \in [0.1, 0.7]; \quad D \in \left[\frac{1}{1000}, \frac{2}{25}\right].$$

$$\sqrt{2}B + 2T \leq 1.$$

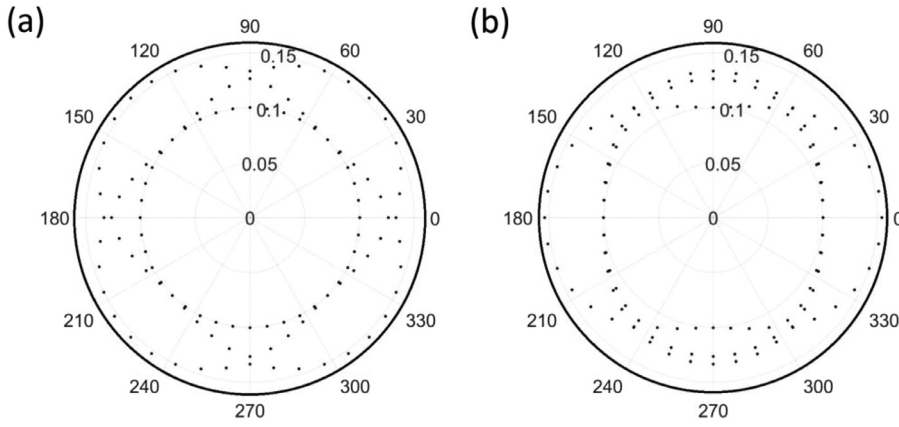


Fig. 8. (a) Polar distribution of phase velocities (m/s) in the X–Y plane of the unit cell. (b) Distribution of phase velocities (m/s) in the plane constructed by vectors (1,1,0) and (0,0,1).

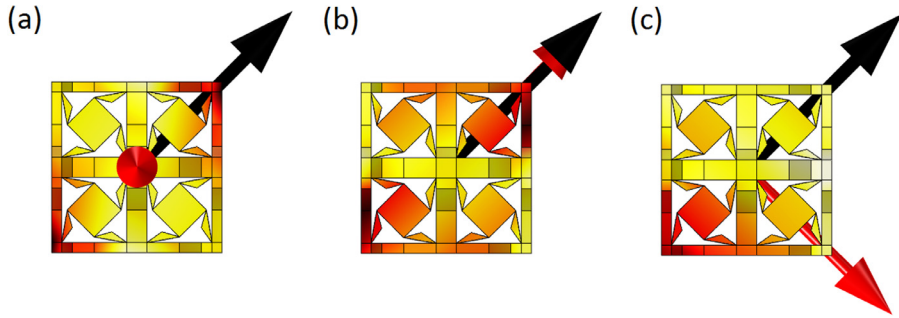


Fig. 9. Eigenmode shapes at (a) 80.3 Hz. (b) 100.8 Hz and (c) 106.1 Hz. The wavenumber $k = 0.1^* \pi/a$. Red arrows represent the direction of displacement, whereas the three modes show clear orthogonal polarization. (For interpretation of the references to color in this figure legend, the reader is referred to the web version of this article.)

And:

$$W_{max} = \frac{\tan(\alpha) + 1}{2 - 2 \tan(\alpha)} * \frac{A - \sqrt{2B - 2T}}{2 \sin(\alpha)}$$

$$\text{where } \alpha = \arctan\left(\frac{1 - \sqrt{2B - 2T}}{1 - 2T}\right)$$

The optimization algorithm is run for 100 iterations, the minimum RMSD is set to $1 * 10^{-4}$ for refined differentiation with the indices ranking. The final parameters are as follow:

$$B = \frac{B}{a} = 0.36218; T = \frac{t}{a} = 0.19126; W = \frac{w}{a} = 0.07604;$$

$$D = \frac{d}{a} = 0.00101.$$

The outcomes are illustrated in Fig. 7.

While the original structure exhibits a complete gap as wide as 21.99%, after 100 iterations of optimization, the final gap width is calculated to be 38.93%. The performance of the mechanical metamaterial, measured by the bandgap width, is increased by 77.04%. The optimized shape is very much similar to that of the original, although deformation such as an enlarged thickness can be observed as indicated by the geometric parameters.

Fig. 8 depicts the phase velocities and their dependency on the orientation of the wave vector. The symmetrical results are as expected from a cubic unit cell. Although the phase velocities show an anisotropic distribution, the four-fold symmetry in the X–Y plane coincides with that in the original design.

Following the polar representation, the phase velocity in the ΓM direction is investigated to retrieve the value of Poisson’s ratio. Here we selected the first three eigenmodes, which showed orthogonal polarization in the displacement vector. The mode shapes are depicted as follows in Fig. 9.

Utilizing both the longitudinal eigenmode and the transverse eigenmodes the Poisson’s ratio is calculated from the phonon band structure. At low frequencies this dynamic result approximates the static estimation. Considering the elasticity tensor \bar{C} , the following derivations are

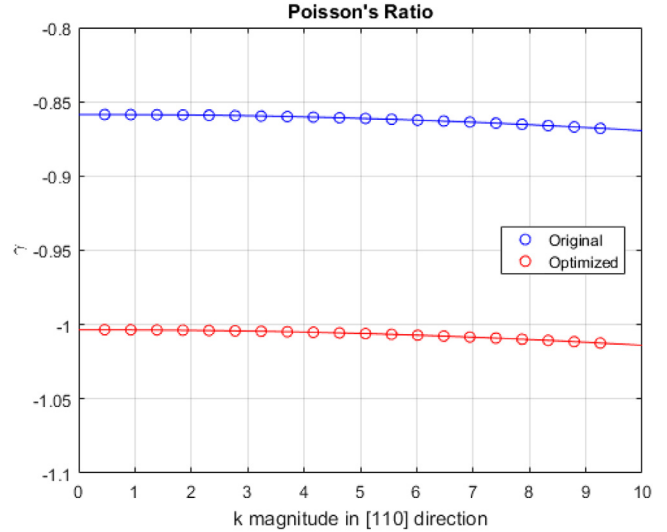


Fig. 10. The dynamic approximation of Poisson’s ratio. The blue and red curves represent the original and optimized models. Values of the ratio are determined by retrieving the polarized phase velocities at various frequencies. (For interpretation of the references to color in this figure legend, the reader is referred to the web version of this article.)

given:

$$C_{44} = \rho \left(v_{110}^{T,z} \right)^2, C_{12} = \rho \left(v_{110}^L \right)^2 - C_{44} - \rho \left(v_{110}^{T,xy} \right)^2, C_{11} = 2\rho \left(v_{110}^{T,xy} \right)^2 + C_{12}.$$

Where the non-zero components in the tensor, C_{11} , C_{12} and C_{44} , can be determined from the polarized phase velocities. Following this, the Poisson’s ratio is easily calculated:

$$\gamma = \frac{C_{12}}{C_{11} + C_{12}}.$$

Here the low frequency region is selected, as indicated by small wave numbers to provide an approximation of the static case. The results from both geometry patterns are shown in Fig. 10. In comparison to the original proposed by Buckmann et al., the optimized geometry yields a Poisson's ratio of -1.0034 . This is calculated by taking a polynomial fit to the phonon band structure data. Using the same method the original Poisson's ratio is determined to be -0.8586 . The decrease in the negative Poisson's ratio is resulted from a decreased d/a ratio, as suggested in the original work. And the optimized result coincides with the trend demonstrated within.

4. Conclusion

Inspired by the previous study on mechanical metamaterial structures that possess wave manipulation capabilities, this work is dedicated to exploring the potential of shape optimization by means of numerical optimization algorithm. Particularly the Nelder–Mead simplex method is incorporated with FEA calculations to evaluate and improve the objective value, which is simply the relative band gap width as extracted from the band structure plotted by the eigenfrequency solver.

With repetitive trials with both two-dimensional and three-dimensional models, the NM method has proven to be very effective and efficient in optimizing the shape of metamaterial structures. This study reveals the capabilities of the NM method in operating within multi-variable parameter domain. The NM method harbors great potential in improving the performance of mechanical metamaterial structures proposed previously, and shall be utilized more frequently. Based on the findings of this work one can expect the Nelder–Mead method to be further explored with more existing mechanical metamaterial designs. New methods will be developed with more stability and the efficiency of this method, as compared to other optimization methods, will also be further evaluated over more iterations.

Supplementary materials

Supplementary material associated with this article can be found, in the online version, at doi:10.1016/j.enganabound.2019.03.011.

References

- [1] Liu Z, Zhang X, Mao Y, Zhu YY, Yang Z, Chan C T, et al. Locally resonant sonic materials. *Science* 2000;289(5485):1734–6.
- [2] Babae S, Shim J, Weaver J C, Chen E R, Patel N, Bertoldi K. 3D soft metamaterials with negative Poisson's ratio. *Adv Mater* 2013;25(36):5044–9.
- [3] Bückmann T, Schittny R, Thiel M, Kadic M, Milton G W, Wegener M. On three-dimensional dilational elastic metamaterials. *New J Phys* 2014;16(3):033032.
- [4] Schaedler T A, Jacobsen A J, Torrents A, Sorensen A E, Lian J, Greer J R, et al. Ultralight metallic microlattices. *Science* 2011;334(6058):962–5.
- [5] Mecklenburg M, Schuchardt A, Mishra Y K, Kaps S, Adelung R, Lotnyk A, et al. Aerographite: ultralightweight, flexible nanowall, carbon microtube material with outstanding mechanical performance. *Adv Mater* 2012;24(26):3486–90.
- [6] Kadic M, Bückmann T, Stenger N, Thiel M, Wegener M. On the practicability of pentamode mechanical metamaterials. *Appl Phys Lett* 2012;100(19):191901.
- [7] Fokin V, Ambati M, Sun C, Zhang X. Method for retrieving effective properties of locally resonant acoustic metamaterials. *Phys Rev B* 2007;76(14):144302.
- [8] Silverberg J L, Evans A A, McLeod L, Hayward R C, Hull T, Santangelo C D, et al. Using origami design principles to fold reprogrammable mechanical metamaterials. *Science* 2014;345(6197):647–50.
- [9] Wang T, Sheng M-P, Qin Q-H. Multi-flexural band gaps in an Euler–Bernoulli beam with lateral local resonators. *Phys Lett A* 2016;380(4):525–9.
- [10] Chang Z, Guo H-Y, Li B, Feng X-Q. Disentangling longitudinal and shear elastic waves by neo-Hookean soft devices. *Appl Phys Lett* 2015;106(16):161903.
- [11] Lakes R. Foam structures with a negative Poisson's ratio. *Science* 1987;235:1038–40.
- [12] Friis E A, Lakes R S, Park J B. Negative Poisson's ratio polymeric and metallic foams. *J Mater Sci* 1988;23(12):4406–14.
- [13] Pennec Y, Vasseur J O, Djafari-Rouhani B, Dobrzyński L, Deymier P A. Two-dimensional phononic crystals: examples and applications. *Surf Sci Rep* 2010;65(8):229–91.
- [14] Lucklum F, Vellekoop M J. Design and fabrication challenges for millimeter-scale three-dimensional phononic crystals. *Crystals* 2017;7(11):348.
- [15] Baz A. The structure of an active acoustic metamaterial with tunable effective density. *New J Phys* 2009;11(12):123010.
- [16] Zhou J, Dong J, Wang B, Koschny T, Kafesaki M, Soukoulis C M. Negative refractive index due to chirality. *Phys Rev B* 2009;79(12):121104.
- [17] Yang S, Page J H, Liu Z, Cowan M L, Chan C T, Sheng P. Focusing of sound in a 3D phononic crystal. *Phys Rev Lett* 2004;93(2):024301.
- [18] Lee S H, Park C M, Seo Y M, Wang Z G, Kim C K. Acoustic metamaterial with negative density. *Phys Lett A* 2009;373(48):4464–9.
- [19] Zhang S, Yin L, Fang N. Focusing ultrasound with an acoustic metamaterial network. *Phys Rev Lett* 2009;102(19):194301.
- [20] Yang Z, Mei J, Yang M, Chan N H, Sheng P. Membrane-type acoustic metamaterial with negative dynamic mass. *Phys Rev Lett* 2008;101(20):204301.
- [21] Mei J, Ma G, Yang M, Yang Z, Wen W, Sheng P. Dark acoustic metamaterials as super absorbers for low-frequency sound. *Nat Commun* 2012;3:756.
- [22] Bendsøe M P, Díaz A, Kikuchi N. Topology and generalized layout optimization of elastic structures. *Topology design of structures*. Springer; 1993. p. 159–205.
- [23] Yamamoto T, Maruyama S, Nishiwaki S, Yoshimura M. Topology design of multi-material soundproof structures including poroelastic media to minimize sound pressure levels. *Comput Methods Appl Mech Eng* 2009;198(17–20):1439–55.
- [24] Donofrio M. Topology optimization and advanced manufacturing as a means for the design of sustainable building components. *Procedia Eng* 2016;145:638–45.
- [25] Gao F, Han L. Implementing the Nelder–Mead simplex algorithm with adaptive parameters. *Comput Optim Appl* 2012;51(1):259–77.
- [26] Luersen M A, Rodolphe Le Riche, Globalized Nelder–Mead method for engineering optimization. *Comput Struct* 2004;82(23–26):2251–60.
- [27] Dennis JE, Woods D J. Optimization on microcomputers: the Nelder–Mead simplex algorithm. *New Comput Environ: Microcomput Large-Scale Comput* 1987;11:6–122.
- [28] Olsson D M, Nelson L S. The Nelder–Mead simplex procedure for function minimization. *Technometrics* 1975;17(1):45–51.
- [29] Lagarias J C, Reeds J A, Wright P E. Convergence properties of the Nelder–Mead simplex method in low dimensions. *SIAM J Optim* 1998;9(1):112–47.
- [30] Qin QH, Wang H. Matlab and C programming for Trefftz finite element methods. New York: CRC Press; 2009.
- [31] Qin QH. Hybrid-Trefftz finite element method for Reissner plates on an elastic foundation. *Comput Methods Appl Mech Eng* 1995;122(3–4):379–92.
- [32] Qin QH. Hybrid Trefftz finite-element approach for plate bending on an elastic foundation. *Appl Math Model* 1994;18(6):334–9.
- [33] Qin QH. Variational formulations for TFEM of piezoelectricity. *Int J Solids Struct* 2003;40(23):6335–46.